Geophysical Journal International

Geophys. J. Int. (2013) **194,** 524–533
Advance Access publication 2013 April 17

doi: 10.1093/gji/ggt114

On microseisms recorded near the Ligurian coast (Italy) and their relationship with sea wave height

G. Ferretti,[1,*] A. Zunino,[2] D. Scafidi,[1] S. Barani[1] and D. Spallarossa[1]

[1]*Seismological Laboratory, Dipartimento di Scienze della Terra, dell'Ambiente e della Vita, University of Genoa, Genoa, Italy.*
E-mail: ferretti@dipteris.unige.it
[2]*Department of Applied Mathematics and Computer Science, Technical University of Denmark, Copenhagen, Denmark*

Accepted 2013 March 20. Received 2013 March 13; in original form 2011 December 16

SUMMARY

In this study, microseism recordings from a near coast seismic station and concurrent significant sea wave heights ($H_{\frac{1}{3}}$) are analysed to calibrate an empirical relation for predicting sea wave height in the Ligurian Sea. The study stems from the investigation of the damaging sea storms occurred in the Ligurian Sea between 2008 October and November. Analysing data collected in this time frame allows identification of two types of microseism signal, one associated to the local sea wave motion and one attributable to a remote source area. The former is dominated by frequencies greater than 0.2 Hz and the latter by frequencies between 0.07 and 0.14 Hz. Moreover, comparison of microseism spectrogram and significant sea wave heights reveals a strong correlation in that the spectral energy content of microseism results proportional to the sea wave height observed in the same time window. Hence, an extended data set including also observations from January to December 2011 is used to calibrate an empirical predictive relation for sea wave height whose functional form is a modified version of the classical definition of $H_{\frac{1}{3}}$. By means of a Markov chain Monte Carlo algorithm we set up a procedure to investigate the inverse problem and to find a set of parameter values for predicting sea wave heights from microseism.

Key words: Time-series analysis; Numerical solutions; Inverse theory; Probabilistic forecasting.

1 INTRODUCTION

Microseisms, small- and long-continuing seismic signals unrelated to earthquakes but caused by natural events, have been observed and studied since the 19th century (Bertelli 1872). They are characterized by periods between about 2 and 40 s. Such low frequency seismic noise has been interpreted as short-period *P* waves, higher mode of surface waves, long-period surface waves and ultra-long-period surface waves (e.g. Gutenberg 1947; Rhie & Romanowicz 2004; Gerstoft & Tanimoto 2007). As pointed out by many authors (e.g. Haubrich *et al.* 1963), most of microseismic energy is in the form of Rayleigh waves and its spectrum is strongly related to ocean wave energy coupling into the Earth motion. Analysis of the relationship between microseisms and ocean waves has a long history, dating back to the first half of 1900, when Lee (1935) published a study on the direction of approach of microseism waves, relating large microseisms to storms and variations of pressure in weather maps. Later, in the 1950s, Longuet-Higgins (1950) solved the excitation process of microseism pointing out that the excitation mechanism of large-amplitude secondary peak microseisms at about 5–7 s is related to the dominant period of ocean waves, at about 10–14 s (in case of relatively closed seas, as the Mediterranean, the range of wave periods is generally limited up to around 8 s). In the same period, Darbyshire (1950) observed that nearby and distant sources may originate microseismic waves characterized by different predominant frequencies. More recently, the study of microseism has concerned different topics among which it is worth mentioning (1) the characterization of low-frequency ambient noise levels (McNamara *et al.* 2004; Chevrot *et al.* 2007), (2) high-resolution surface wave ambient noise tomography (Shapiro *et al.* 2005) and (3) the analysis of the relationship between microseism and sea waves, analysis of climate change and planning shore protection measures (Grevemeyer *et al.* 2000; Bromirski *et al.* 2005; Tanimoto *et al.* 2006; Stutzmann *et al.* 2009). Several studies have shown that microseisms can be detected in the pressure field of the oceans by deep-ocean acoustic measurements, employing, for instance, ocean bottom seismometers (e.g. Duennebier *et al.* 2012). These microseisms have the same features than signals recorded onshore except for amplitude, which results strongly weakened. For this reason, seismic stations located near the coast record more energetic signals. Recently, Ardhuin *et al.* (2011) presented the first comprehensive numerical modelling of microseism, valid for global ocean and based on random ocean waves generation furthermore taking into account coastal reflections. Generally, two types of microseisms can be observed and distinguished (e.g. Cessaro 1994; Barruol *et al.*

* DipTeRis

2006). The primary microseism is generated by direct ocean wave pressure variations on the ocean bottom (in shallow seafloor) and has the same frequency as the generating ocean waves (Hasselmann 1963). This mechanism is effective only in shallow water because the amplitude of pressure fluctuations decreases exponentially from the free surface to the sea bottom, thereby the level of primary microseism may result undetectable. The frequency content of primary microseism spans from 0.05 to 0.1 Hz. The secondary microseism is dominated by a frequency that is approximately twice the ocean wave frequency (the so called double-frequency). Its origin has been explained by the theory of Longuet-Higgins (1950): the interaction of two equal wavelength ocean waves travelling in opposite direction generates second-order pressure fluctuations on the ocean floor with double frequency. These waves propagate with very low attenuation and then turn into microseismic energy. The frequency content of secondary microseism ranges from 0.1 to 0.5 Hz. Although it cannot be generalized to all areas, the secondary microseism may be further divided into long period microseism (0.085–0.2 Hz), which is due to far away sources (e.g. swell from distant storms), and short period microseism (0.2–0.5 Hz), which is due to sources located near the coast (e.g. waves induce by local wind) (Stephen *et al.* 2003; Bromirski *et al.* 2005). The frequency corresponding to the sea wave spectrum peak varies with the sustained wind speed and the size of the fetch, decreasing when the wind speed increases (Sverdrup & Munk 1947; Pierson & Moskowitz 1964). The level of the noise source is a function of the directional wave spectrum, which contains the amplitude information of the interacting waves and, again, results from the characteristics of wind fields, coastal reflections and currents (Hasselmann 1963; Ardhuin *et al.* 2011).

In this paper, we first focus on featuring the spectral properties of microseism recorded by a seismic station located near the Ligurian Sea coast during a particular sea storm in late 2008. This force-ten sea storm, which was sustained by a wind speed up to 27 m s^{-1} (around 52 knots, measured by an anemometer belonging to the University of Genoa), caused several troubles to the dock and the airport of Genoa and produced significant damages along the coast. The comparison of the microseism spectrogram with the significant sea wave height recorded by a buoy near Côte d'Azur (France) has evidenced a strong correlation. Hence, based on an extended data set including also data measured between 2011 January (hereafter referred as Jan) and to 2011 December (hereafter referred as Dec) by the Côte d'Azur buoy (data from other buoys in the Ligurian Sea were not available), we have developed a law to predict sea wave heights as a function of the power spectral density (PSD) of the vertical component of microseism. A Markov chain Monte Carlo method has been employed to solve this inverse problem and finally to calibrate the predictive law for the Ligurian Sea. The potential of our model is tested by comparing predicted sea wave height values with observed data recorded in a period of time different from that covered by the data set used for the calibration of the model.

2 CHARACTERISTICS OF MICROSEISM BETWEEN 2008 OCTOBER AND NOVEMBER

2.1 Data and processing

Microseism data recorded by a broad-band seismic station (IMI, Imperia) belonging to the Regional Seismic network of Northwestern Italy (RSNI network, www.dipteris.unige.it/geofisica) from October (hereafter referred as Oct) 25 to 2008 November (hereafter referred as Nov) 19 are compared with a concurrent data set of sea wave heights measured by the Côte d'Azur buoy (latitude 43.38, longitude 7.83, depth of anchoring 2300 m, see Fig. 1) which belongs to the Météo-France network (www.meteo.shom.fr). The IMI station stands close to the French border, at few tenths of kilometres from the coastline, at the foot of the Alps. Its position makes this station particularly suitable for analysing microseism in that the storms occurring in the Ligurian Sea are well imaged in seismic signals recorded very close to the sea, with low attenuation (Marzorati & Bindi 2008). The time frame analysed in this section includes several meteo-marine events. In particular, during Oct 30–31 a major sea storm, which caused several damages and is clearly distinguishable in the data (Fig. 2), occurred.

Microseismic data recorded by IMI consist of three-component velocimetric recordings with a sampling frequency of 100 Hz. We processed the seismic data following this scheme:

(i) instrumental correction (deconvolution);
(ii) signal resampling at a frequency of 2 Hz;
(iii) offset and linear trend removal;
(iv) signal windowing into 1 hr windows (according to buoy data sampling);
(v) computation of the Fourier transform of each window;
(vi) spectrogram calculation and
(vii) estimation of microseism polarization (as explained in the following).

2.2 Microseism spectral analysis and correlation with sea wave height

The significant wave height is employed here as reference parameter to quantify sea wave height. It is defined (Sverdrup & Munk 1947) as the mean of the one third highest heights (measured over the time period T) and is calculated from the wave elevation variance, which is also the zero moment (m_0) of a non-directional wave spectrum, using

$$H_{\frac{1}{3}} = 4\sqrt{m_0}, \tag{1}$$

where m_0 is given by

$$m_0 = \int_{f_{\min}}^{f_{\max}} \frac{2}{T}|S(f)|^2 \mathrm{d}f \tag{2}$$

in which $\frac{2}{T}|S(f)|^2$ is the PSD of sea waves, $f_{\min}$ and $f_{\max}$ are the minimum and maximum frequencies of integration.

Fig. 2 compares microseism spectral characteristics with sea wave heights. Taken as a whole Fig. 2 allows us to appreciate the relation between microseism spectrogram, significant sea wave heights, and the frequency of sea waves (again obtained from the Côte d'Azur buoy). Specifically, the spectrogram in Fig. 2(a) shows the amplitude Fourier spectrum of the vertical component of the microseism recording as a function of time. Note that time windows containing teleseisms (i.e. earthquakes located at a great distance from the seismic station) with a magnitude greater than 6.0 as reported in the bulletin of the Centre Sismologique Euro-Méditerranéen (www.emsc-csem.org/Earthquake) were removed from recordings.

During the whole period Oct 25–Nov 19, two meteo-marine phenomena (indicated as type 'A' and type 'B' in Fig. 2a) occurred altering strongly the spectral characteristics of the seismic recordings, mainly for frequencies below 0.5 Hz (Fig. 2a). These phenomena are identified by marked variations in the sea wave height values measured at the buoy (Fig. 2b). Type 'A' phenomena, which include three microseismic events labeled as 'A1' (Oct 25–28), 'A2'

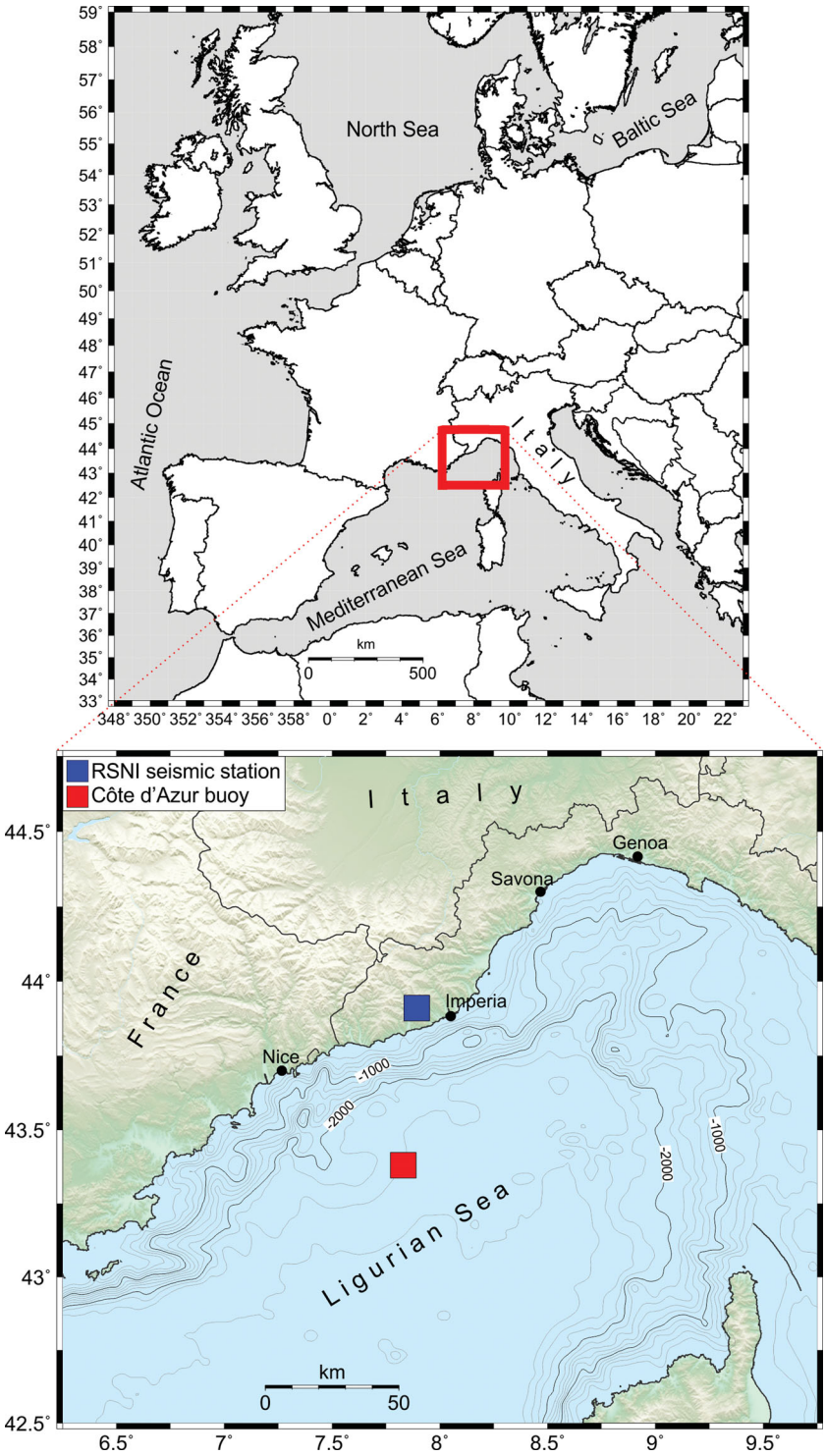

Figure 1. Geographical location of the area under study. The position of the IMI (Imperia) seismic station and of the Côte d'Azur buoy is shown by blue and red squares.

(Nov 7–12), and 'A3' (Nov 16–19) in Fig. 2(a), are characterized by mild sea wave heights (lower than approximately 1.5 m). In the period Oct 25–28 ('A1' event), two peaks appear in the frequency band 0.05–0.2 Hz. They are centred on 0.07 and 0.14 Hz (see also Fig. 3a) and can also be seen in the Nov 7–12 and 16–19 periods ('A2' and 'A3' events, respectively), as depicted in Fig. 2(a). Type 'B' phenomena, which may be related to local storms occurred in the Ligurian Sea during the periods Oct 29–Nov 6 and Nov 13–15, present wave heights up to 3.7 m and include two microseismic events ('B1' and 'B2' in Fig. 2a). In particular, during Oct 29–Nov 6 ('B1' event) the 0.14 and 0.07 Hz peaks are almost completely attenuated and maximum amplitudes concentrate at about 0.2–0.3 Hz. The 'B1' event can be further divided into three subevents that are indicated in the spectrogram as 'B1a', 'B1b' and 'B1c' (Fig. 2a). 'B1a' (approximatively Oct 30–31) is the most energetic and peaks at the lowest frequency (around 0.2 Hz). 'B1b' (Nov 2–3) presents

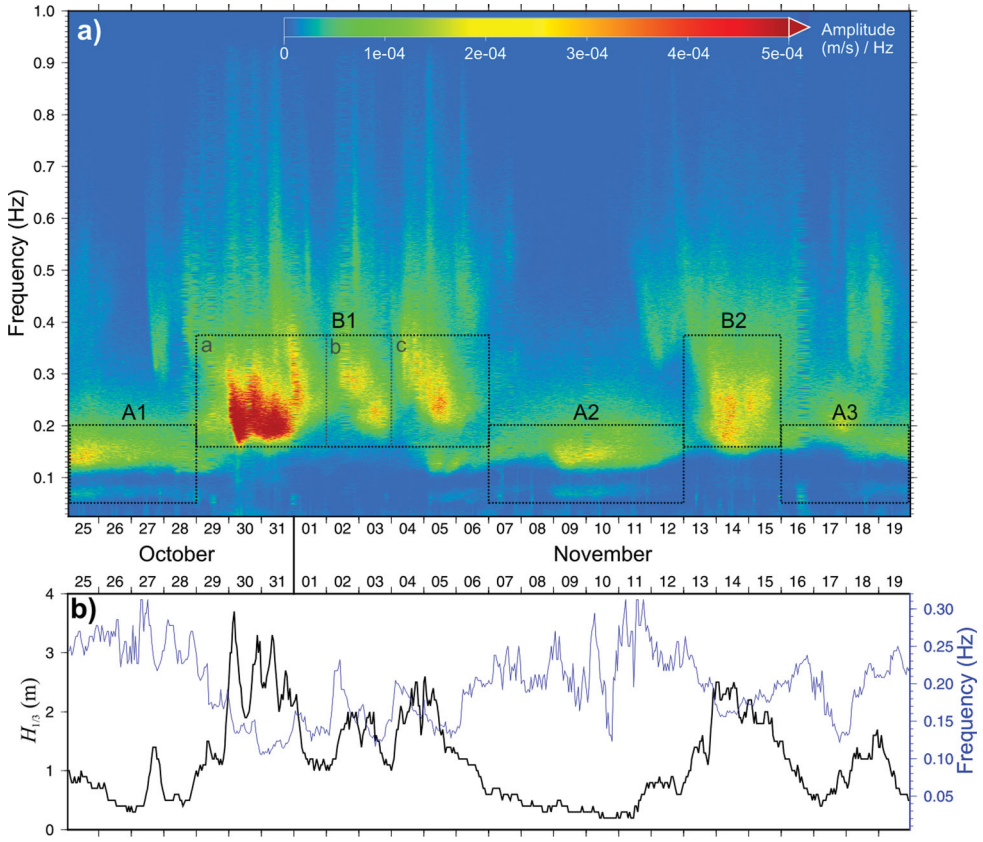

Figure 2. Correlation between microseism and measured sea wave parameters. (a) Spectrogram of the vertical component of the microseism recorded from 2008 October 25 to 2008 November 19. The colour scale represents the amplitude of the Fourier spectrum computed over windows of 1 hr (see text for details); (b) significant sea wave height (black line) and sea wave frequency (blue line) versus time as measured by the Côte d'Azur buoy. Dashed boxes indicate type 'A' and type 'B' microseismic phenomena (see the text for details).

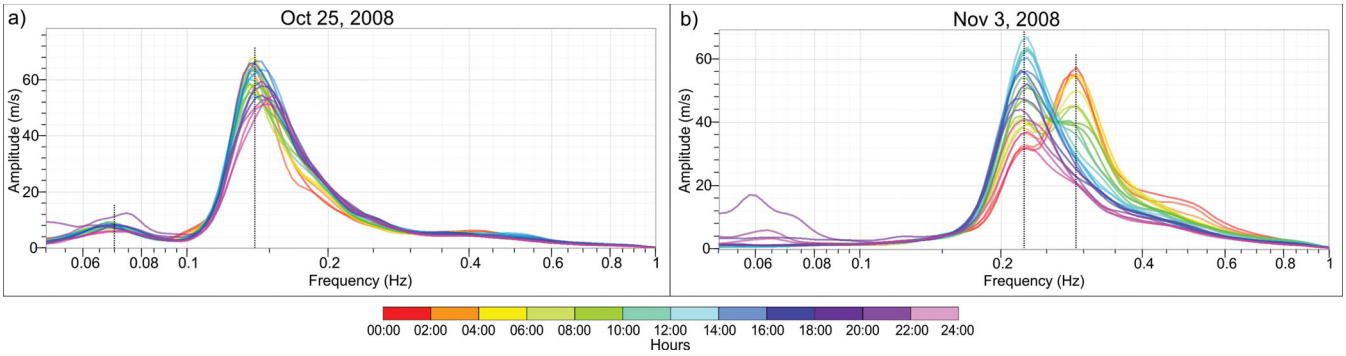

Figure 3. Hourly amplitude Fourier spectra (normalized to the duration of the signal) of the microseism recorded during 2008 October 25 (a) and the 2008 November 3, Ligurian Sea storm (b). The colour bar indicates the time window of each spectrum. The dotted vertical lines indicate the high amplitude peaks discussed in the text.

two distinct high amplitude areas characterized by different frequencies, as evidenced by the spectrogram. Of note, on Nov 3 (Fig. 3b), a particular behaviour can be observed. In that day, the prevailing frequency of microseism moves from about 0.3 to 0.2 Hz with the highest sea wave heights occurring during the beginning of the day, when the microseism features higher frequencies. Specifically, during the morning, the sea wave frequency measured at the buoy (blue line in Fig. 2b) is around 0.16 Hz, the microseism peaks at 0.28 Hz, and the significant sea wave height (black line in Fig. 2b) spans from 1.7 to 2 m. In the afternoon, the sea wave frequency drops to about 0.13 Hz, the microseism peak shifts down to 0.22 Hz, and the wave height gradually decreases to 1.1 m. Note that the sea wave frequency values used here are average data reported by the buoy and, therefore, they may be approximately 25 per cent larger than the true peak frequencies obtainable from the sea wave spectrum (not available). This frequency decrease with time is also observable for the 'B1c' subevent (Nov 4–6), which is slightly more energetic than 'B1b', and for the 'B2' event (Nov 13 and Nov 15).

Summarizing previous observations, it is evident that a strong correlation between the microseismic signal and the significant wave height exists, in that the energy of the microseism increases with sea wave height. The most energetic events in the amplitude spectrum (Fig. 2a) are reflected in the values of $H_{\frac{1}{3}}$ (Fig. 2b). As an example, the major storm event occurred in the period Oct 30–31 is

clearly imaged both in the microseism spectrum and the sea wave height plots. Analogous observations can be made focusing on the following two sea storm episodes (Nov 2–3, Nov 4–6), showing the increase of both microseism spectral amplitude and sea waves height.

Analysing the relation between the microseism spectral content and sea wave frequency (Fig. 2) shows a variable level of correlation. A cross-correlation analysis performed on the data measured by the buoy and the hourly predominant frequency of microseism reveals a high correlation (of approximately 96 per cent) during the time windows Oct 29–Nov 6 and Nov 13–15, when the frequency of sea waves (∼0.11–0.16 Hz) is about half the peak frequency of microseism (∼0.2–0.3 Hz). The correlation level decreases down to around 60 per cent when the whole period of observation (from Oct 25 to Nov 19) is taken into account. Of note, the level of correlation may be slightly underestimated as the mean frequency values of sea waves are used instead of the full buoy spectrum (not available). Indeed, as observed above, the mean frequency values tend to be higher than those derived from the full sea wave spectrum and, as a consequence, the microseism may result to be dominated by frequencies a bit below twice those measured at the buoy.

2.3 Polarization

The polarization of the seismic signal is defined (Tanimoto *et al.* 2006) as the maximum of the quantity I as a function of the angle φ (measured clockwise from north), assuming that Rayleigh waves dominate the microseism:

$$I = \sum_{i=1}^{n} \left[N(\omega)\cos(\varphi) + E(\omega)\sin(\varphi) \right]^2, \tag{3}$$

where $N(\omega)$ and $E(\omega)$ are the (hourly) complex Fourier spectra of the north and east components of recordings. The polarization analysis is performed distinguishing between time windows characterized by mild significant sea wave heights (Oct 25–28, Nov 7–12 and

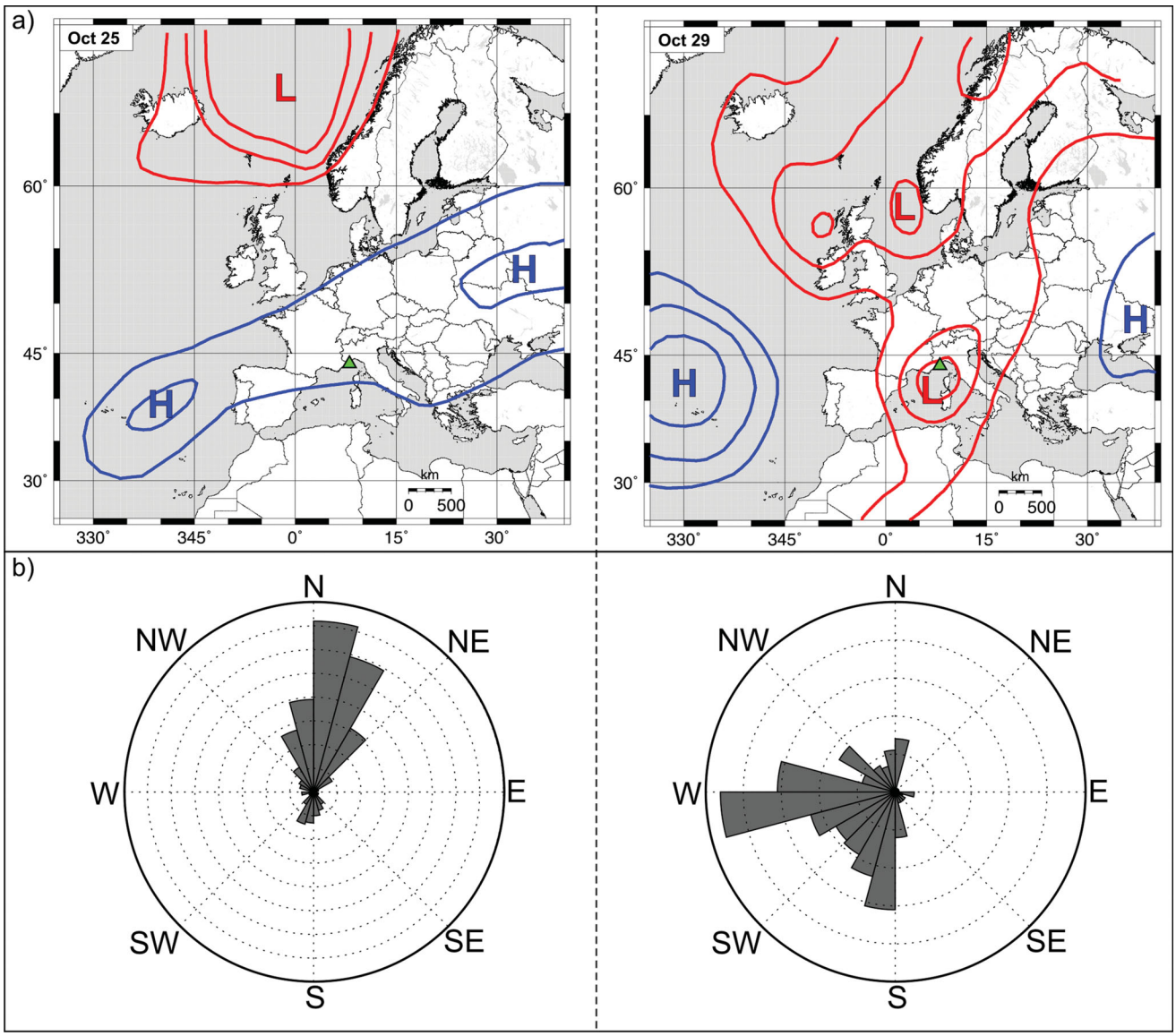

Figure 4. Barometric pressure maps and microseism polarization. (a) Simplified barometric pressure maps (modified from www.eumetsat.int) relative to 2008 October 25 (left-hand panel) and 2008 October 29 (right-hand panel); (b) rose histograms showing the microseism polarization for the periods October 25–28, November 7–12 and November 16–19 (left-hand panel) and for the periods October 29–November 6 and November 13–15 (right-hand panel).

Nov 16–19, Fig. 4b, left-hand panel) and windows presenting wave heights greater than 1.5 m (Oct 29–Nov 6 and Nov 13–15, Fig. 4b, right-hand panel). In both cases, inside each hourly recording window, the predominant frequency is determined from the largest peak observed in the power spectrum of the vertical component (Chevrot *et al.* 2007). The azimuth of the principal horizontal polarization axis is then computed from the spectra in a frequency range of ±0.01 Hz around the predominant frequency (Tanimoto *et al.* 2006). The upper limit of summation in eq. (3), n, is the number of discrete frequencies within ±0.01 Hz. Finally, the property of fundamental mode Rayleigh waves, which present a retrograde particle motion at the surface, is taken into account to remove the 180° ambiguity in azimuth definition, thus making possible the determination of the true incoming direction of microseism (Tanimoto *et al.* 2006; Chevrot *et al.* 2007).

Comparing barometric pressure maps with the polarization plots allows us to discern the effect of different barometric depressions in Europe on microseismic characteristics. According to Darbyshire (1950), who showed that microseismic waves of different periods travel independently and may have different origins, the microseism signal analysed here may be related to different source areas. During the Ligurian storms occurred between Oct 29 and Nov 6, which were caused by a cyclone in the Mediterranean Sea (labelled as 'L' in Fig. 4a) moving from west to east (Fig. 4a, right-hand panel), the microseism is dominated by frequencies greater than 0.2 Hz and presents a variable incoming azimuth spanning from south to west, with a prevalent westward orientation (Fig. 4b, right-hand panel). During the time periods Oct 25–28, Nov 7–12, and Nov 16–19 one may observe that (1) the sea wave heights measured by the buoy are lower than 1.5 m, (2) the microseism is characterized by two frequency peaks at 0.07 and 0.14 Hz and by a predominant N–NNE incoming direction (Fig. 4b, left-hand panel) and (3), concurrently, a deep depression is localized in the Norwegian Sea (Fig. 4a, left-hand panel). Although an accurate location of the microseism source can only be obtained via a broad-band frequency-wavenumber analysis, our previous observations seem to agree with results of several authors working on the localization of microseismic source areas in the Atlantic ocean and Mediterranean Sea. In particular, for the periods Oct 29–Nov 6 and Nov 13–15, our findings agree with results of Chevrot *et al.* (2007) showing the presence of microseismic source areas near the Corsica and Menorca islands. These sources are located south and southeast of the IMI station, respectively. Likewise, for the periods Oct 25–28, Nov 7–12 and Nov 16–19, our polarization results confirm the findings of many authors (e.g. Friedrich *et al.* 1998; Stutzmann *et al.* 2009; Landes *et al.* 2010) evidencing the existence of a microseism source near the north Norwegian coast. Therefore, the microseism dominated by frequency peaks at 0.07 and 0.14 Hz could be ascribed to a source area outside the Ligurian Sea whereas that dominated by frequencies greater than 0.2 Hz could be generated in the Mediterranean Sea. This issue is further discussed in the final section of the article where a cross-correlation analysis between observed and predicted significant sea wave heights is presented.

3 PREDICTION OF SEA WAVE HEIGHT FROM MICROSEISM

The Ligurian Sea basin features a particular shape due to the curved geometry of the coastline and a particular bathymetry presenting a very steep continental slope (see Fig. 1). For this reason, the interaction of sea waves generating the double-frequency microseism may result very complicated, giving rise to complex seismic response. Therefore, since exhaustive modelling may be very difficult to be implemented numerically, our objective in this paper is to develop an empirical model to predict sea wave height as a function of the vertical component of microseism. To this end, we use an extended data set including both recordings from Oct 25 to Nov 19, 2008 and recordings from 2011 Jan 1 to Dec 31. First we test a simple model based on the standard definition of significant sea wave height (eq. 1). Then, analysing the statistical distribution of measured wave heights, we propose a more accurate modelization. Mathematically, the simple model based on eq. (1) is expressed as:

$$H_{\frac{1}{3}}^{\mathrm{calc}} = 4\,c\,\sqrt{\int_{f_{\min}}^{f_{\max}} \frac{2}{T}|S_m(f)|^2 \mathrm{d}f}, \tag{4}$$

where c is a scaling coefficient that adjusts the level of the seismic signal to the sea wave height and $\frac{2}{T}|S_m(f)|^2$ is the PSD of microseism.

To solve for the three unknowns of the model ($f_{\min}$, $f_{\max}$ and c), we developed an *ad hoc* procedure based on an inverse methodology in the framework of the probabilistic approach, originally proposed by Tarantola & Valette (1982). Writing the forward model in the classical form:

$$\mathbf{g}(\mathbf{m}) = \mathbf{d}, \tag{5}$$

where $\mathbf{g}$ is the (possibly) non-linear operator that computes $\mathbf{H}_{\frac{1}{3}}^{\mathrm{calc}} = \mathbf{d}$ given $\mathbf{m}$, our inverse modelling consists in finding the ensemble of models $\mathbf{m} = (f_{\min}, f_{\max}, c)$ which best explain our observations. We assume our uncertainties to be distributed according to a Gaussian probability density function (*pdf*) and set up a Markov chain Monte Carlo algorithm to sample the *a posteriori pdf*:

$$\sigma(\mathbf{m}) = k\,\rho(\mathbf{m})\,L(\mathbf{m}), \tag{6}$$

where k is a normalization constant, $\rho(\mathbf{m})$ represents the *a priori pdf*, and $L(\mathbf{m})$ the likelihood function which gives a measure of the misfit between observed and computed data (Mosegaard & Tarantola 1995). Defining m_{cur} as our current model and m_{pert} as some randomly perturbed model according to the *a priori* information $[\rho(\mathbf{m})]$, the metropolis rule (Hastings 1970) implemented in our algorithm can be summarized as follows:

(i) perturb the current model m_{cur} to obtain m_{pert} (according to the *a priori* distribution);

(ii) accept the perturbed model (m_{pert}) with probability

$$P_{\mathrm{accept}} = \min\left[1, \frac{L(m_{\mathrm{pert}})}{L(m_{\mathrm{cur}})}\right];$$

(iii) if m_{pert} is accepted, set $m_{\mathrm{cur}} = m_{\mathrm{pert}}$ and

(iv) go back to (i).

The peculiarity of the Monte Carlo method is that one obtains an ensemble of solutions consistent with the observations instead of a single solution. The spread of the models obtained may be then used for estimating the range of reasonable values of significant sea wave heights that can be predicted from microseism.

Following Bromirski (2001), we first search for the temporal relationship between microseism and sea wave height values through signal cross-correlation. To this end, $H_{\frac{1}{3}}$ is calculated using eq. (4) and adopting values of $f_{\min}$ and $f_{\max}$ obtained from a preliminar Monte Carlo run. The cross-correlation reveals about a 2 hr delay of microseism with respect to sea wave height. This delay may be ascribed to the particular sea basin characteristics and differences in source–receiver path.

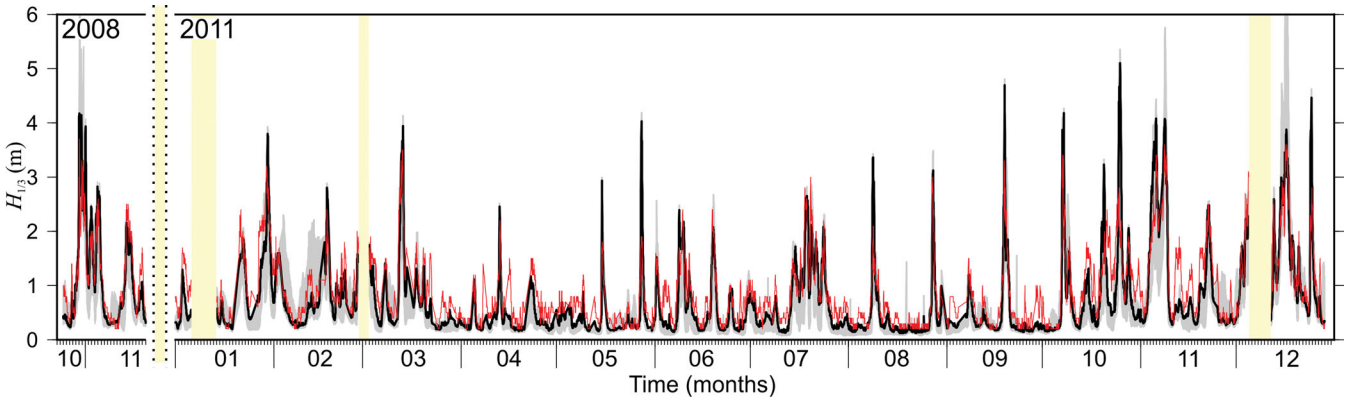

Figure 5. Comparison between the significant sea wave height values measured at the buoy (red line) and those predicted by the 'best-fitting model' based on eq. (4) (black line). The grey lines indicate the family of significant sea wave height predictions obtained from the ensemble of solutions of the inverse problem. Yellow areas indicate periods with missing data.

Finally, to calibrate the predictive model in eq. (4), we apply the Monte Carlo search for $f_{\min}$, $f_{\max}$ and c to the shifted microseism data taking the time of the sea wave heights recorded at the buoy as reference. Running 100 000 iterations, we obtained about 2500 models, representing our set of solutions. To get independent samples, we retained only one every 20 accepted models. Since we search for a single solution to compute the significant sea wave height, the model with the highest likelihood, corresponding to $\mathbf{m} = (f_{\min}, f_{\max}, c) = (0.25, 0.97, 350\,000)$, is chosen as our 'best-fitting model'. Fig. 5 compares the significant sea wave heights recorded at the buoy with the set of $H_{\frac{1}{3}}^{\text{calc}}$ values resulting from the Monte Carlo simulation. The black curve indicates the values of sea wave height predicted by the 'best-fitting model'. The agreement between the two time-series is fairly good both in terms of amplitude (wave heights) and phase, in that no time-shift is present (as proved by a cross-correlation analysis). The average difference between observed and computed wave heights is about 0.26 m. However, some observed sea wave height peaks are strongly overestimated (by more than 1 m) by the predicted values.

Hence, in order to refine the sea wave height prediction, we modify the forward model according to the empirical observation that $H_{\frac{1}{3}}$ follows a lognormal distribution. The hypothesis that the observed data follow a lognormal distribution is proved via a Kolmogorov–Smirnov test which shows that the sample is drawn from the reference (lognormal) distribution assuming a level of significance of 5 per cent. The new predictive model has the following mathematical expression:

$$H_{\frac{1}{3}}^{\text{calc}} = \exp\left(a + b \ln\left(\sqrt{\int_{f_{\min}}^{f_{\max}} \frac{2}{T}|S_m(f)|^2 \mathrm{d}f}\right)\right), \qquad (7)$$

where a, b, $f_{\min}$ and $f_{\max}$ are the four unknowns of the model.

From the ensemble of solutions obtained from a new run of the Monte Carlo algorithm (Fig. 6), we select the 'best-fitting model' corresponding to:

$$\mathbf{m} = (f_{\min}, f_{\max}, a, b) = (0.24, 0.78, 9.48, 0.66).$$

Analogously to Fig. 5, Fig. 7 compares recorded and predicted sea wave height values. Again, the two time-series show a good agreement in terms of phase. However, the new model provides significant sea wave height values that better fit the experimental observations (the average difference between observed and computed wave heights is now reduced to about 0.19 m), overcoming the limitation of the model in eq. (4) which was found to overestimate wave height peaks. Nevertheless, some rare peaks overestimating the observed values are still visible in Fig. 7 (e.g. the largest overestimation, of 1.75 m, is detectable near the end of October 2011; however, observed values are overestimated by more than 1 m in 0.7 per cent of cases and by more than 1.5 m four times only). As observed by Ardhuin *et al.* (2012), such outliers may be ascribed to particular events that, for a same wave height, happen to be much more noisy. These sporadic events, which originate when two wave systems of distinct origin but equal wave periods run into one another, are classified as Class III events by Ardhuin *et al.* (2012). Moreover, a few slightly underestimated peaks (underestimated by no more than around 0.5 m) are also visible. This underestimation may be ascribed to the predictive model that does not take into account the contribution of the microseism for frequencies lower than 0.24 Hz, thus neglecting the maximum amplitudes of the spectrogram observed during the main local storms in the Ligurian Sea (see Fig. 2a).

4 DISCUSSION AND CONCLUSIONS

A strong correlation between microseism recordings and sea wave data is well known since long time. In this work, we showed that this holds also true for the Ligurian Sea analysing a data set that includes the microseism recorded by a near-coast seismic station and concurrent significant sea wave heights from a buoy. Hence, by using a procedure based on a Markov chain Monte Carlo algorithm, we obtain an empirical law to predict the significant sea wave height as a function of the vertical component of microseism. Analysing the amplitude Fourier spectrum of microseism recordings has pointed out the variability of the frequencies dominating microseism. Distinction can be made between microseism controlled by frequencies of 0.07 and 0.14 Hz (hereinafter low-frequency microseism) and microseism with dominating frequencies of around 0.2–0.3 Hz (hereinafter high-frequency microseism). The former is generally accompanied by moderate sea wave heights (up to around 1.5 m). The latter may be associated to local storms producing sea wave heights up to around 4 m. These findings, in conjunction with results from the polarization analysis showing that low- and high-frequency microseisms are characterized by different polarization directions, would suggest the double origin of the microseism recorded in the Ligurian Sea. Hence, to prove that different microseism spectral

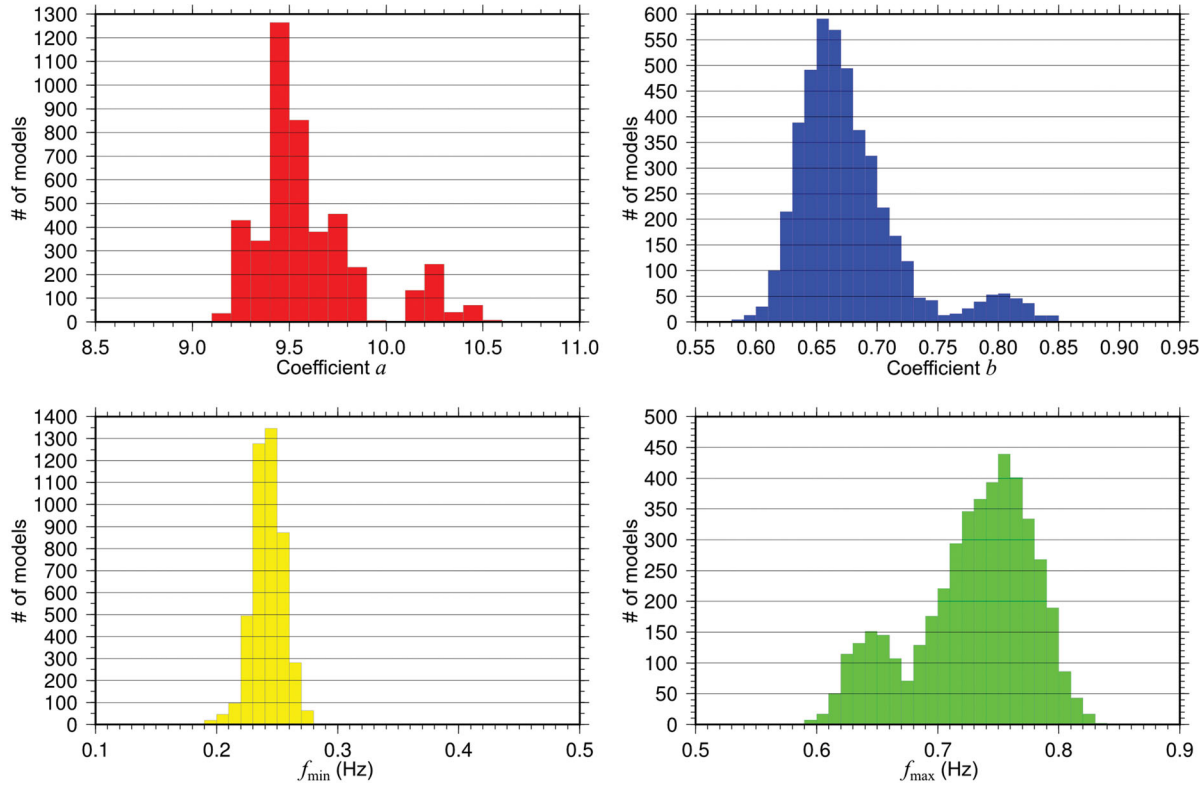

Figure 6. Frequency distributions of the coefficients in eq. (7) as derived from the Monte Carlo search.

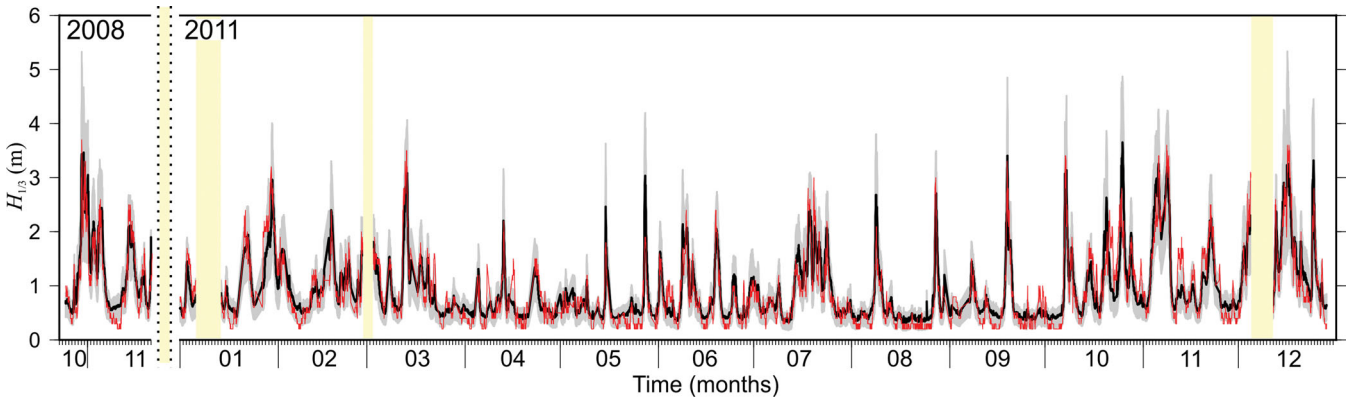

Figure 7. Comparison between the significant sea wave height values measured at the buoy (red line) and those predicted by the 'best-fitting model' based on eq. (7) (black line). The grey lines indicate the family of significant sea wave height predictions obtained from the ensemble of solutions of the inverse problem. Yellow areas indicate periods with missing data.

characteristics (e.g. dominating frequencies) are representative of different microseism sources, we compute the cross-correlation between measured sea wave heights and wave heights predicted by the model in eq. (7) for different values of f_{min} and f_{max}, which were defined based on the spectral analysis presented in Section 2.2 (see also the spectrogram in Fig. 2a). Specifically, assuming $f_{min} = 0.01$ Hz and $f_{max} = 0.15$ Hz, the signals show a correlation of 64 per cent. A higher level of correlation (87 per cent) was reached assuming $f_{min} = 0.15$ Hz and $f_{max} = 0.4$ Hz. Obviously, the highest correlation (93 per cent) was found using the values of f_{min} and f_{max} obtained from the numerical inversion ($f_{min} = 0.24$ Hz and $f_{max} = 0.78$ Hz). Therefore, the lower degree of correlation obtained using $f_{min} = 0.01$ Hz and $f_{max} = 0.15$ Hz suggests that the low-frequency microseism could be ascribed to a source area outside the Ligurian Sea, as also hypothesized from the polarization analysis.

In order to test the predictive power of the empirical model derived in this study, model which is applicable only in the Ligurian Sea area, we compare the predicted sea wave heights with those measured by the Côte d'Azur buoy in the period 2012 January 01–February 11 (Fig. 8). Fig. 8 clearly displays a good agreement between the observed and predicted values. The average difference between them is around 0.21 m.

Concluding, our findings indicate that reliable estimates of the sea wave height in the Ligurian Sea may be predicted from microseism data recorded near the coast. Although the study is based on data from a single buoy only, the predictive law derived here can be confidently applied to predict significant sea wave heights in the area under study. Indeed, a variety of storms of different size, location and intensity were included in the data set used for the model calibration. Future research based on a larger set of recordings

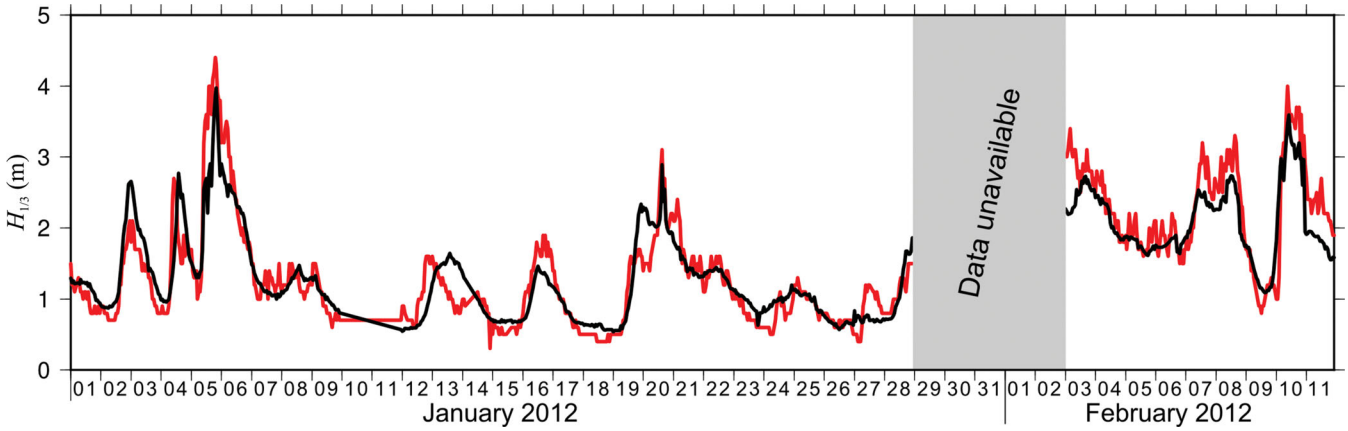

Figure 8. Comparison between the significant sea wave heights measured at the buoy (red line) during 2012 January 01 and 2012 February 11 and the predicted values computed by applying the 'best-fitting model' based on eq. (7) (black line). The IMI station was not in operation between 2012 January 29 and 2012 February 02.

from different buoys and seismic stations may help in improving further the predictive power of the model, possibly extending its applicability to a larger area. However, as observed by Ardhuin *et al.* (2012), the application to larger areas requires the basic knowledge of the distribution of the microseisms sources and of the crust properties (which influence seismic wave attenuation).

ACKNOWLEDGEMENTS

This work has been made using the data provided by the Côte d'Azur buoy that belongs to the Centre de Météorologie Marine (CMM) of Météo-France. In particular, we are grateful to Gilbert Emzivat, Jöel Quere, Jean Rolland (Météo-France) and Jean-Paul Jullien for their support in providing us the buoy data. We wish to thank Prof Claudio Eva for encouraging this study and for his fruitful suggestions. Last but not least, we are thankful to four anonymous reviewers for their thorough review and useful comments that improve this article.

REFERENCES

Ardhuin, F., Stutzmann, E., Schimmel, M. & Mangeney, A., 2011. Ocean wave sources of seismic noise, *J. geophys. Res.,* **116,** C09004, doi:10.1029/2008JC005215.

Ardhuin, F., Balanche, E., Stutzmann, E. & Obrebski, M., 2012. From seismic noise to ocean wave parameters: general methods and validation, *J. geophys. Res.,* **117,** C05002, doi:10.1029/2011JC007449.

Barruol, G., Reymond, D., Fontaine, F.R., Hyvernaud, O., Maurer, V. & Maamaatuaiahutapu, K., 2006. Characterizing swells in the southern Pacific from seismic and infrasonic noise analyses, *Geophys. J. Int.,* **164,** 516–542.

Bertelli, T., 1872. Osservazioni sui piccoli movimenti dei pendoli in relazione ad alcuni fenomeni meteorologiche, *Boll. Meteorol. Osserv. Coll. Roma,* **9**.

Bromirski, P.D., 2001. Vibrations from the "Perfect Storm", *Geochem. Geophys. Geosys.,* **2,** doi:10.1029/2000GC000119.

Bromirski, P.D., Duennebier, F.K. & Stephen, R.A., 2005. Mid-ocean microseisms, *Geochem. Geophys. Geosyst.,* **6,** Q04009, doi:10.1029/2004GC000768.

Cessaro, R.K., 1994. Sources of primary and secondary microseisms, *Bull. seism. Soc. Am.,* **84,** 142–148.

Chevrot, S., Sylvander, M., Benahmed, S., Ponsolles, C., Lefèvre, J.M. & Paradis, D., 2007. Source locations of secondary microseisms in western Europe: evidence for both coastal and pelagic sources, *J. geophys. Res.,* **112,** B11301, doi:10.1029/2007JB005059.

Darbyshire, J., 1950. Identification of microseismic activity with sea waves, *Proc. R. Soc. Lond. A,* **202,** 438–448.

Duennebier, F.K., Lucas, R., Nosal, E-M., Aucan, J. & Weller, R.A., 2012. Wind, waves, and acoustic background levels at Station ALOHA, *J. geophys. Res.,* **117,** C03017, doi:10.1029/2011JC007267.

Friedrich, A., Krüger, F. & Klinge, K., 1998. Ocean-generated microseismic noise located with Gräfenberg array, *J. Seismol.,* **2,** 47–64.

Gerstoft, P. & Tanimoto, T., 2007. A year of microseisms in southern California, *Geophys. Res. Lett.,* **34,** L20304, doi:10.1029/2007GL031091.

Grevemeyer, I., Herber, R. & Essen, H.H., 2000. Microseismological evidence for a changing wave climate in the northeast Atlantic Ocean, *Nature,* **408,** 349–352.

Gutenberg, B., 1947. Microseisms and weather forecasting, *J. Atmos. Sci.,* **4,** 21.

Hasselmann, K., 1963. A statistical analysis of the generation of microseisms, *Rev. geophys. Space Phys.,* **1,** 177–210.

Hastings, W.K., 1970. Monte Carlo sampling methods using Markov chains and their applications, *Biometrika,* **57,** 97–109.

Haubrich, R.A., Munk, W.H. & Snodgrass, F.E., 1963. Comparative spectra of microseisms and swell, *Bull. seism. Soc. Am.,* **53,** 27–37.

Landes, M., Hubans, F., Shapiro, N.M., Paul, A. & Campillo, M., 2010. Origin of deep ocean microseisms by using teleseismic body waves, *J. geophys. Res.,* **115,** B05302, doi:10.1029/2009JB006918.

Lee, A.W., 1935. On the direction of approach of microseismic waves, *Proc. R. Soc. Lond., A,* **149,** 183–199.

Longuet-Higgins, M.S., 1950. A theory of the origin of microseisms, *R. Soc. Lond. Philos. Trans. Ser. A,* **243,** 1–35.

Marzorati, S. & Bindi, D., 2008. Characteristics of ambient noise cross correlations in Northern Italy within the frequency range of 0.1–0.6 Hz, *Bull. seism. Soc. Am.,* **98,** 1389–1398.

McNamara, D.E. & Buland, R.P., 2004. Ambient noise levels in the continental United States, *Bull. seism. Soc. Am.,* **94,** 1517–1527.

Mosegaard, K. & Tarantola, A., 1995. Monte Carlo sampling of solutions to inverse problems, *J. geophys. Res.,* **1001,** 12 431–12 448.

Pierson, W.J. & Moskowitz, L., 1964. A proposed spectral form for fully developed wind seas based on the similarity theory of S. A. Kitaigorodskii, *J. geophys. Res.,* **69,** 5181–5190.

Rhie, J. & Romanowicz, B., 2004. Excitation of Earth's continuous free oscillations by atmosphere-ocean-seafloor coupling, *Nature,* **431,** 552–556.

Shapiro, N.M., Campillo, M., Stehly, L. & Ritzwoller, M.H., 2005. High-Resolution surface-wave tomography from ambient seismic noise, *Science,* **307,** 1615–1618.

Stephen, R.A., Spiess, F.N., Collins, J.A., Hildebrand, J.A., Orcutt, J.A., Peal, K.R., Vernon, F.L. & Wooding, F.B., 2003. Ocean seismic network pilot experiment, *Geochem. Geophys. Geosyst.,* **4,** 1–38.

Stutzmann, E., Schimmel, M., Patau, G. & Maggi, A., 2009. Global climate imprint on seismic noise, *Geochem. Geophys. Geosyst.,* **101,** Q11004, doi:10.1029/2009GC002619.

Sverdrup, H.U. & Munk, W.H., 1947. Wind, sea and swell. Theory of relations for forecasting, *U.S. Navy Hydrographic Office, Washington, Pub. No. 601,* 44 pp.

Tanimoto, T., Ishimaru, S. & Alvizuri, C., 2006. Seasonality in particle motion of microseisms, *Geophys. J. Int.,* **166,** 253–266.

Tarantola, A. & Valette, B., 1982. Generalized nonlinear inverse problems solved using the least squares criterion, *Rev. geophys. Space Phys.,* **20,** 219–232.